Armin Sigmund and Riqo Chaar contributed equally to this work.

A Case Study on Drivers of the Isotopic Composition of Water Vapor at the Coast of East Antarctica

Armin Sigmund[1] , Riqo Chaar[1] , Pirmin Philipp Ebner[2,3], and Michael Lehning[1,2]

[1]School of Architecture, Civil and Environmental Engineering, CRYOS, EPFL, Lausanne, Switzerland, [2]WSL Institute for Snow and Avalanche Research SLF, Davos, Switzerland, [3]Now at Geophysical Institute and Bjerknes Centre for Climate Research, University of Bergen, Bergen, Norway

Abstract Stable water isotopes (SWIs) contain valuable information on the past climate and phase changes in the hydrologic cycle. Recently, vapor measurements in the polar regions have provided new insights into the effects of snow-related and atmospheric processes on SWIs. The purpose of this study is to elucidate the drivers of the particularly depleted vapor isotopic composition measured on a ship close to the East Antarctic coast during the Antarctic Circumnavigation Expedition in 2017. Reanalysis data and backward trajectories are used to model the isotopic composition of air parcels arriving in the atmospheric boundary layer (ABL) above the ship. A simple model is developed to account for moisture exchanges with the snow surface. The model generally reproduces the observed trend with strongly depleted vapor δ^{18}O values in the middle of the 6-day study period. This depletion is caused by direct air mass advection from the ice sheet where the vapor is more depleted in heavy SWIs due to distillation during cloud formation. The time spent by the air masses in the marine ABL shortly before arrival at the ship is crucial as ocean evaporation typically leads to an abrupt change in the isotopic signature. Snow sublimation is another important driver when the isotopic composition of the sublimation flux differs substantially from that of the advected air mass, for example, marine air arriving at the coast or free-tropospheric air descending from high altitudes. Despite strong simplifications, our model is a useful and computationally efficient method for understanding SWI dynamics at polar sites.

Plain Language Summary Stable water isotopes are useful to reconstruct historical temperature conditions from ice cores. This method is possible because phase changes of water alter the isotopic composition. For example, if an air mass cools down, forms clouds, and produces rain or snowfall, the water vapor preferentially loses heavy water molecules. This study aims to explain a remarkable vapor isotopic signal measured on a ship close to the East Antarctic coast during 6 days in 2017. We model the isotopic composition of air parcels along their pathways to the ship and develop a novel approach to represent moisture exchange with the snow surface. The modeled vapor isotopic composition at the ship reaches a distinct minimum, similar to the measurements, when the air parcels move directly from the ice sheet to the ship. As expected, the vapor isotopic composition is lower over the ice sheet than over the ocean, largely due to cloud formation. However, moisture uptake from the snow surface and from the ocean shortly before arrival at the ship can strongly and abruptly influence the isotopic signature of the air masses. Although our model is not perfect, it helps to improve the interpretation of isotope measurements at polar sites.

1. Introduction

Stable water isotopes (SWIs) are widely used as both tracers in the global hydrologic cycle (Elliot, 2014; Koeniger et al., 2010) and as climate proxies in ice cores (EPICA community members, 2004; Grootes et al., 1994; Lorius et al., 1979). The isotopic composition (δ^{18}O or δD) describes the abundance of a heavy water isotopologue (H_2^{18}O or HD^{16}O) in a water sample, in relation to a standard as defined in Text S1 of Supporting Information S1. The heavy isotopologues contain stronger molecular bonds than the light isotopologue, H_2^{16}O, which leads to slight differences in the saturation vapor pressure of the isotopologues (e.g., Jancso et al., 1970; Matsuo & Matsubaya, 1969). Therefore, the solid phase is generally more enriched in SWIs than the liquid phase and, to a stronger degree, than the vapor phase. This effect is known as equilibrium fractionation. Phase changes in natural conditions such as ocean evaporation can additionally be associated with kinetic fractionation, resulting from the fact that the heavy isotopologues have lower molecular diffusivities in air than the light isotopologue (e.g., Jouzel & Merlivat, 1984). Kinetic fractionation will play a relevant role if the phase change occurs at a fast rate. This will

be the case if a strong vertical humidity gradient enhances ocean evaporation, which is typical in the cold sector of extratropical cyclones (Thurnherr et al., 2021).

The isotopic compositions of water vapor and snow are affected by several processes, starting from ocean evaporation in the moisture source region (Craig & Gordon, 1965; Merlivat & Jouzel, 1979), transport processes in the atmosphere (Helsen et al., 2006), cloud formation and precipitation (Ciais & Jouzel, 1994; Jouzel & Merlivat, 1984), and postdepositional processes at and below the snow surface (Cuffey & Steig, 1998; Helsen et al., 2005, 2007; Johnsen et al., 2001; Jouzel et al., 2003; Krinner & Werner, 2003). When an air mass experiences more and more cloud formation, the fractionation effects give rise to isotopic distillation of atmospheric vapor. As a result, snowfall and surface snow on the Antarctic Ice Sheet generally become more depleted in heavy SWIs with increasing distance from the coast and elevation (Masson-Delmotte et al., 2008).

Isotopic fractionation also plays an important role in phase changes at the Earth's surface. These phase changes influence air masses transported in the atmospheric boundary layer (ABL) as this layer is typically well mixed by turbulence and thus affected by surface-atmosphere interactions. While the fractionation effects are well understood in the case of ocean evaporation, they are subject of current research in the case of snow sublimation. Traditionally, it was assumed that sublimation occurs layer by layer without fractionation (Friedman et al., 1991; Neumann & Waddington, 2004; Town et al., 2008). More precisely, it was argued that self-diffusion in ice is slow enough such that the snow layer affected by sublimation would transform completely into vapor before being mixed with the snow layer underneath. Consequently, the average isotopic composition of the sublimation flux would equal the initial isotopic composition of the sublimating snow layer. However, recent experimental studies found evidence of fractionation during sublimation. For example, Hughes et al. (2021) sampled near-surface vapor and snow in northeast Greenland with a high temporal resolution on clear-sky summer days and compared the isotope dynamics with sublimation measurements. These observations demonstrated that alternating periods of sublimation and vapor deposition can lead to clear diurnal cycles in the vapor isotopic composition, which are consistent with changes in the snow isotopic composition. Similar diurnal cycles in the vapor isotopic composition were reported for Dome C on the Antarctic plateau and explained by local sublimation and vapor deposition (Casado et al., 2016). These findings are supported by controlled experiments in cold laboratories, showing that snow-vapor exchange at the surface and in the pore space alters the isotopic compositions of snow and vapor (e.g., Ebner et al., 2017; Sokratov & Golubev, 2009). Equilibrium fractionation explains a large part of these SWI dynamics although the measurements indicate some influence of kinetic fractionation (Casado et al., 2016; Hughes et al., 2021; Wahl et al., 2021).

The influence of kinetic fractionation is often assessed using deuterium excess, also called d-excess and defined as $\delta D - 8\, \delta^{18}O$ (Dansgaard, 1964). This definition is motivated by the fact that most precipitation samples from across the world lie, on average, on a line with a slope of 8 in the δD-$\delta^{18}O$ diagram, which agrees approximately with the classic Rayleigh distillation model for an air mass cooling from 20 to $-20°C$ with an initial vapor isotopic composition in equilibrium with ocean water. This model describes condensation assuming equilibrium fractionation and an immediate removal of the liquid or solid water phase. While kinetic fractionation changes the d-excess value, equilibrium fractionation is generally expected to have a negligible effect on this value. However, Dansgaard (1964) notes that the δD-$\delta^{18}O$ relationship for a specific precipitation event depends on several parameters, including the initial vapor isotopic composition, initial temperature, and condensation temperature. These dependencies imply that equilibrium fractionation can influence d-excess in certain conditions. For example, the classic Rayleigh distillation model predicts the d-excess of snowfall to increase significantly when reaching very low temperatures and very depleted isotopic compositions, which are typical for the Antarctic plateau (e.g., Dütsch et al., 2017; Touzeau et al., 2016).

The isotopic composition of atmospheric vapor observed at a specific polar site is influenced by weather changes on different time scales. At Thule Air Base, coastal northwest Greenland, Akers et al. (2020) observed a strong seasonal cycle in vapor isotopic composition controlled by shifts in sea-ice extent, which define the distance to marine moisture sources. Synoptic weather events led to variations over multiple days, superimposed on the seasonal cycle. At Syowa station, coastal East Antarctica, Kurita et al. (2016a) also found a strong influence of synoptic weather systems, causing advection of marine or glacial air masses with distinct isotopic signatures. At other coastal polar sites, shifts between these air masses manifest themselves in pronounced diurnal cycles in the vapor isotopic composition, at least in summertime high-pressure periods. An example is Dumont d'Urville, coastal East Antarctica, where strong katabatic winds advect dry air with strongly depleted $\delta^{18}O$ values from

the interior of the ice sheet during the coldest hours of the day (Bréant et al., 2019). Similar diurnal cycles can be observed at Kangerlussuaq, southwest Greenland, where an ice-free strip of land alternatingly experiences katabatic winds and a see breeze (Kopec et al., 2014).

Apart from measurements, models are an important tool for understanding the dynamics of SWIs in the atmosphere and the driving processes. There are two modeling approaches: (a) Lagrangian models which simulate moist processes and isotopic fractionation along air parcel trajectories (Christner et al., 2017; Ciais & Jouzel, 1994; Helsen et al., 2006; Jouzel & Merlivat, 1984; Sinclair et al., 2011); and (b) Eulerian models, such as general circulation models (GCMs), which consider the temporal change on a fixed three-dimensional grid (e.g., Joussaume et al., 1984; Pfahl et al., 2012). Eulerian models provide a more accurate representation of the spatial variability of the isotopic composition of water vapor across the hydrologic cycle by accounting for the mixing of air masses of different origins and the highly variable pathways water vapor may take between evaporation and condensation. For example, GCMs are able to satisfactorily reproduce the global and seasonal variations in the isotopic composition of precipitation (Hoffmann et al., 2000; Noone & Sturm, 2010). However, it is more difficult to discern the effect of individual processes on isotopic variability using Eulerian models as these processes can be isolated less easily, compared to the computationally more efficient Lagrangian models (Dütsch et al., 2018). Thurnherr et al. (2021) used a combination of both approaches to better understand vapor isotopic measurements along the ship route of the Antarctic Circumnavigation Expedition (ACE). The output of the Eulerian model COSMO$_{iso}$ was analyzed along backward trajectories starting at the position of the ship. This method demonstrated that the cold and warm sectors of extratropical cyclones, associated with evaporation and dew formation, respectively, were important drivers of the vapor isotopic composition over the open ocean.

The ACE campaign also provided insights into meridional SWI variations in the ABL of the Atlantic and the Southern Ocean (Thurnherr, Kozachek, et al., 2020). From November 2016 to April 2017, continuous SWI time series were recorded on the ship as it traveled from Germany via South Africa to Antarctica and back. The vapor was generally more depleted in heavy SWIs with distance from the tropics, reflecting average patterns in temperature and specific humidity and their influence on the fractionation processes.

In the present study, we develop a Lagrangian model to explain the vapor isotopic signal of a specific event during the ACE campaign. We investigate in detail a 6-day period in January 2017, in which the ship stayed close to the Mertz glacier, East Antarctica, and the values of vapor $\delta^{18}O$ reached a pronounced minimum. The objectives are to (a) reproduce the $\delta^{18}O$ values of water vapor observed at the Mertz glacier using a Lagrangian model with simple isotope dynamics and (b) better understand the influences of air mass origin and isotopic fractionation during moisture exchange with the Earth's surface and during cloud formation. Our model accounts for equilibrium fractionation but neglects kinetic effects during all phase changes apart from ocean evaporation. As some other models still neglect isotopic fractionation during snow sublimation, we analyze how sensitive the modeled vapor $\delta^{18}O$ is with respect to the assumptions that snow sublimation is or is not associated with equilibrium fractionation. Although our model represents some processes less accurately than the COSMO$_{iso}$-based modeling framework of Thurnherr et al. (2021), we are able to directly distinguish the effects of individual processes with a lower computational effort. The main novelty of our isotope model is the fact that the isotopic composition of sublimating surface snow is computed by accounting for the history of snowfall and surface-atmosphere exchange. This computation represents the first modeling step, which is performed in an Eulerian frame of reference, considering a multi-layer snowpack. The last aspect is an advantage over the COSMO$_{iso}$ model, which treats the snowpack as a single homogeneous layer. As sublimation and vapor deposition affect primarily the uppermost few centimeters of the snowpack and sustained sublimation may uncover deeper snow layers, a realistic description of the isotopic composition of snow may require the approach of a multi-layer snowpack.

2. Data and Methods

2.1. Water Vapor Measurements at the Mertz Glacier

The ACE expedition involved many research projects in multiple disciplines such as atmospheric chemistry and physics (e.g., Schmale et al., 2019) and oceanography (e.g., Sieber et al., 2019). The vapor isotopic measurements were performed on the ship at heights of approximately 8 and 13.5 m a.s.l. using PICARRO cavity ring-down laser spectrometers with a high temporal resolution of 1 s (Thurnherr, Kozachek, et al., 2020). Most of the time, the isotopic composition was slightly more depleted at the upper height, compared with the lower height, and a
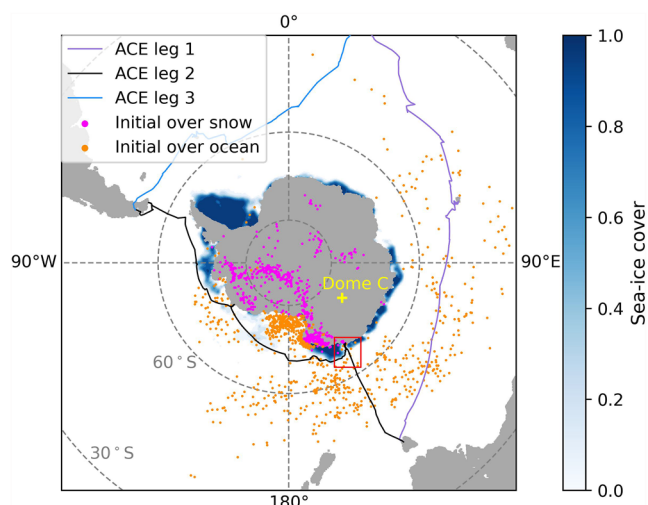
Figure 1. Map showing the three legs of the ship track (solid lines) of the Antarctic Circumnavigation Expedition, average sea-ice cover (blue colors) in the period from 17 January 2017 to 1 February 2017, initial locations of the modeled air parcels (dots), and location of Dome C (yellow cross). The red rectangle highlights the ship track in the study period (close to the Mertz glacier).

strong correlation was found between both heights. We follow the aforementioned authors and focus on the measurements at the upper height, which are less influenced by sea spray. More details and an overview of the measured time series can be found in the aforementioned article.

The ship track around Antarctica can be divided into three legs (Figure 1). Here, we focus on a small section of leg 2 in the proximity of the outlet of the Mertz glacier, East Antarctica, corresponding to the 6-day period from 27 January to 1 February 2017. This period includes two consecutive days with exceptionally depleted values of $\delta^{18}O$ and δD, compared with the remaining time series. The event coincided with low values of specific humidity and high values of d-excess (Figure 5 in Thurnherr, Kozachek, et al. (2020)), typical of continental Antarctic interior air masses (e.g., Bréant et al., 2019).

2.2. Modeling Approach

We developed a model, which considers the most common three SWIs ($H_2^{16}O$, $H_2^{18}O$, $HD^{16}O$). The model consists of two parts: (a) *Model Sublimation* uses an Eulerian frame of reference to compute the isotopic composition of surface snow, which determines that of the sublimation flux; (b) *Model Air Parcel* uses a Lagrangian frame of reference to quantify the vapor isotopic composition along air parcel trajectories, considering vapor exchange with the snow or ocean surface and vapor removal due to cloud formation (Figure 2). First, Model Sublimation is run with a spin-up period of approximately 6 months to allow for the development of realistic snow isotopic compositions. Subsequently, the output of Model Sublimation is used in Model Air Parcel when the air parcel takes up water vapor from the snow surface, that is, when the parcel is located in the ABL and the snow is sublimating. For the phase changes of sublimation, vapor deposition, and condensation, we only consider equilibrium fractionation as a first-order approximation and use temperature-dependent formulas for the fractionation factors from Merlivat and Nief (1967), Majoube (1970), and Majoube (1971). To evaluate the importance of fractionation during sublimation, we compare two simulations, which assume that snow sublimation is associated with equilibrium fractionation (Run E) or not associated with any fractionation (Run N). In both simulations, kinetic fractionation is only taken into account in the process of ocean evaporation by applying the widely used Craig-Gordon formula in its original form (Craig & Gordon, 1965; Horita et al., 2008).
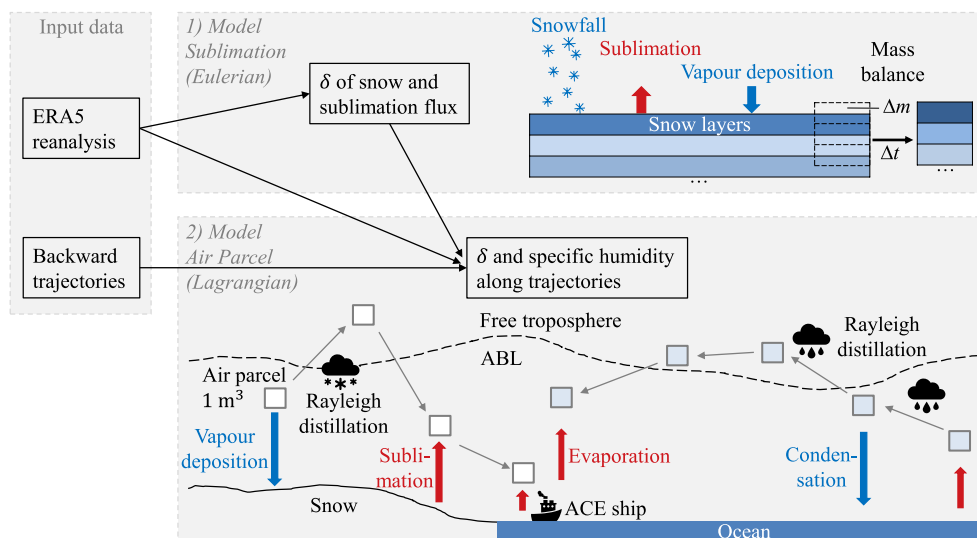

Figure 2. Schematic illustration of the modeling approach. The net accumulation of snow mass in one time step (Δt), denoted by Δm, may be positive or negative.

The next sections explain the input data and main characteristics of the two model parts while further methodological details and equations can be found in Texts S1–S3 of Supporting Information S1. Important model constants and parameters are listed in Table S1 of Supporting Information S1. For brevity, we refer to the surface water vapor flux as the surface flux from here on. All time information in this paper is given in UTC time while local time at the outlet of the Mertz glacier corresponds to UTC + 10 hr.

2.2.1. Input Data

The model uses ERA5 reanalysis data produced by the European Centre for Medium-Range Weather Forecasts (ECMWF) with spatial and temporal resolutions of $0.25° \times 0.25°$ and 1 hr, respectively (Hersbach et al., 2018). The following variables were retrieved: land-sea mask, mean evaporation rate, air temperature and dew point temperature at 2 m height, surface temperature, atmospheric pressure, snowfall rate, and sea-ice cover. The mean evaporation rate characterizes both ocean evaporation and snow sublimation and is based on the common Monin-Obukhov bulk parameterization, assuming constant roughness lengths on the ice sheet ($z_{0m} = 0.0013$ m, $z_{0T} = z_{0q} = 0.00013$ m) and dynamic roughness lengths for the ocean depending on a wave model (ECMWF, 2016). In addition to the snow surface, drifting and blowing snow particles contribute to the sublimation flux (Sigmund et al., 2022) and consequently they may change their isotopic composition. However, drifting and blowing snow is not represented in the ERA5 reanalysis and there is little knowledge about isotopic effects of this process. In the main analysis, we use data for latitudes south of 30°S from July 2016 to February 2017. The first six months serve as a spin-up period to reduce uncertainties arising from the initialization of the snow isotopic composition. For purposes of validation, we compare results of Model Sublimation with isotope measurements at Dome C, East Antarctica, published by Casado et al. (2016, 2018). To this end, ERA5 data for the grid cell including Dome C (75°S, 123.25°E) and the period from January 2013 to January 2016 are used.

Model Air Parcel additionally assimilates 10-day backward air parcel trajectories taken from Thurnherr, Wernli, and Aemisegger (2020). These trajectories were calculated with the Lagrangian analysis tool LAGRANTO (Sprenger & Wernli, 2015; Wernli & Davies, 1997) using the 3D-wind fields from the ECMWF operational analyses. Every hour, a set of trajectories was launched from up to 56 vertical levels between 0 and 500 hPa above sea level along the ACE cruise track. For each trajectory, the time step was 3 hr. In this study, the following variables were extracted for trajectories arriving in the ABL above the ship in the period from 27 January to 1 February 2017: air pressure at heights of the air parcel and the ABL, specific humidity, and air temperature.

2.2.2. Model Sublimation

The isotopic composition of the sublimation flux depends on that of the surface snow (e.g., Wahl et al., 2021). The latter is initialized with typical values for snowfall depending on the temperature and then computed prognostically. The effects of snowfall, sublimation, and vapor deposition on the snow isotopic composition are simulated with time in each grid cell, which is considered as snow-covered land (land fraction >50% and latitude south of 60°S). Model Sublimation uses a time step of 1 hr and simulates the period from 1 July 2016 to 1 February 2017 in the main analysis.

The snowfall $\delta^{18}O$ is parameterized as a linear function of the daily running mean air temperature because in the literature, this relationship is derived from daily mean values. We apply the same linear function to snowfall over the whole Antarctic continent although different $\delta^{18}O$-temperature slopes have been measured at different sites. In our baseline simulation, the function for snowfall $\delta^{18}O$ is taken from Stenni et al. (2016) and characterized by an intermediate slope of 0.45‰ K^{-1}. Sensitivity tests are performed using functions from Landais et al. (2012) and Fujita and Abe (2006) with low and high slopes of 0.35‰ K^{-1} and 0.78‰ K^{-1}, respectively (Texts S2, S4, and S5 in Supporting Information S1). The δD value of snowfall is always derived using the δD-$\delta^{18}O$ relationship of Masson-Delmotte et al. (2008) based on mean isotopic compositions of snow, firn, or ice at many Antarctic sites (Equation 10 in Supporting Information S1).

The snowpack is modeled as a series of 100 layers, each with the same thickness and a constant density of 350 kg m^{-3}. This density does not account for the natural spatiotemporal variability but represents a typical average value for the uppermost tens of centimeters of the snowpack (e.g., Wever et al., 2022). For the location of Dome C, we tested three values for the snow layer thickness (0.1, 1, and 2 cm) and compared the surface snow $\delta^{18}O$ with measurements of Casado et al. (2018). A thickness of 1 cm led to a good agreement and was therefore selected for the remaining analysis (Text S4 and Figure S1 in Supporting Information S1). We assume that the snowpack always exists on the Antarctic Ice Sheet, that is, in grid cells south of 60°S with a land fraction greater

than 50%. If the snowfall and surface fluxes add or remove snow mass at the surface, a simple mixing mechanism will guarantee that the thickness and mass of the snow layers remain constant. More precisely, a part of each layer is mixed with an adjacent layer to compensate for the mass gain or loss at the surface (Figure 2). We neglect changes in snow density and assume that snow added by snowfall or vapor deposition has the same density as the snowpack. The mixing mechanism is a vastly simplified version of a realistic vapor transport mechanism (Jafari et al., 2020). In reality, the interplay between ventilation, isotope diffusion within the snowpack, and recrystallization can cause a continuous replacement of the interstitial water vapor in the surface snow layer. However, it is still an open question how the combination of these processes can quantitatively change the isotopic compositions of snow and water vapor in the ABL. Therefore, our model is based on the following assumptions: (a) no isotope diffusion within the snow layers; (b) no impact of snow metamorphism on the isotopic profile; (c) fractionation only at the uppermost snow layer because of its direct contact with the atmosphere; and (d) no ventilation within the snow layer.

The deposition flux forms surface hoar with an isotopic composition that depends on the isotopic composition of the atmospheric vapor. Model Sublimation estimates the isotopic composition of the atmospheric vapor as the mean of two hypothetical values, describing two idealized situations. In the first situation, the vapor is formed by local snow sublimation and thus characterized by the isotopic composition of the sublimation flux, which differs between Runs E and N. In the second situation, the vapor originates from a non-local source region and has undergone isotopic distillation. This effect is expressed by assuming the vapor to be in isotopic equilibrium with snowfall. We apply this parametrization regardless of whether snowfall occurs at the location and time of interest or not. The snowfall isotopic composition is estimated as a simple function of the daily running mean air temperature, as described above.

The highly parametrized estimate of the vapor isotopic composition is only used to compute the effect of a limited amount of vapor deposition in Model Sublimation and to initialize some air parcels in Model Air Parcel. In reality, however, the relative importance of local and non-local vapor origins is expected to vary depending on the weather conditions. Locally sourced vapor is typically abundant in clear-sky conditions in austral summer because solar radiation enhances sublimation by heating the snow surface. On the contrary, surface cooling in austral winter or in the coldest hours of the day can cause vapor deposition although the intensity of this flux is generally lower than that of the sublimation flux. Additionally, marine air intrusions in coastal areas can lead to events of vapor deposition as warm and moist air is cooled by the snow surface. Nevertheless, vapor deposition at the snow surface plays a limited role in our main analysis because the total mass removed from all modeled air parcels due to vapor deposition is 46 times lower than the total mass taken up by all parcels due to snow sublimation. On the contrary, vapor deposition is relevant in a validation and sensitivity study with Model Sublimation at Dome C (Text S4 in Supporting Information S1). This site is located in the interior of the Antarctic Ice Sheet where the particularly cold atmosphere can only take up a small amount of water vapor, limiting sublimation and increasing the relative importance of vapor deposition. The ERA5 data suggests that vapor deposition outweighs sublimation at Dome C with a net surface flux of 2.7 kg m^{-2} yr^{-1} in the years of 2013–2015. Figure S2b in Supporting Information S1 shows that, if using Run E, the highly parametrized estimate for vapor δ^{18}O reproduces the mean value measured by Casado et al. (2016) at Dome C in a 24-day period in austral summer 2014/2015 (mean bias error of $-0.2‰$) although the temporal variability is strongly underestimated. This comparison suggests that Run E uses a reasonable first-order approximation of the vapor isotopic composition with uncertainties of a few ‰ for δ^{18}O. On the contrary, Run N leads to vapor δ^{18}O values, which are clearly more enriched than the measurements (mean bias error of 10.8‰).

2.2.3. Model Air Parcel

We consider air parcels with a constant volume of $1 \times 1 \times 1$ m^3, traveling along the trajectories that are located in the ABL when reaching the position of the ship. This criterion is met if the air pressure is higher at the location of the trajectory than at the top of the boundary layer. The pressure at the top of the ABL is taken from the trajectory data set and based on ECMWF operational forecasts. As a result, we select 6 to 24 trajectories per arrival time (13 trajectories on average). The surface of each grid cell is represented by one of four surface types: (a) ice-free ocean if the land fraction is ≤50% and the sea-ice cover is ≤90%, (b) snow-covered sea ice if the land fraction is ≤50% and the sea-ice cover is higher than 90%, (c) snow-covered land if the land fraction is higher than 50% and the latitude is south of 60°S, and (d) snow-free land if the land fraction is higher than 50% and the latitude is north of 60°S.

The somewhat arbitrary threshold for sea ice is rather high (90%) because the ocean water is typically warmer and contributes more strongly to the surface flux, compared to a snow surface of the same area. On the contrary, the threshold for the land-sea boundary is set to 50% to be consistent with the modeling approach of the ERA5 data set. A more sophisticated treatment of sea ice could theoretically be implemented by dividing the evaporation flux into contributions from the ice-free ocean and snow-covered sea ice. Yet, the relative contributions do not correspond to the fractions of surface area. As any assumption on the relationship between the flux contribution and area fraction would be arbitrary, we choose the simple threshold approach to account for areas with the strongest impact of sea ice.

The air parcels are not always initialized 10 days before arriving at the ship. Instead, the time of initialization equals the first time at which the trajectory is located in the ABL and the following two restrictions are respected: (a) Over the ice-free ocean, evaporation must occur at the time and location of initialization; (b) the air parcels are not allowed to travel through the ABL over snow-free land because there, the isotopic composition of the surface flux is not known. If these restrictions prevent the initialization, the model will select the next possible time, meeting the criteria. Restriction (a) allows us to estimate the initial isotopic composition of the parcel using the Craig-Gordon formula simplified with the global closure assumption (e.g., Dar et al., 2020). Under this assumption, the isotopic composition of atmospheric vapor over the ocean equals that of the evaporation flux.

If the initialization occurs over snow-covered land or sea ice, the isotopic composition of the parcel will be initialized as a function of the isotopic compositions of surface snow and snowfall (same assumption as used in Model Sublimation for atmospheric vapor). It is challenging to model the isotopic composition of snow on top of sea ice, especially because it can be influenced by sea spray (Bonne et al., 2019). Apart from that, Model Sublimation is not applicable to snow-covered sea ice because a spin-up period of several months will not make sense if the sea-ice area changes with time. As a first-order approximation, Model Air Parcel assumes that the isotopic composition of surface snow above sea ice equals that of the nearest grid cell with snow-covered land at any time of the simulation. An overview of the locations of initialization and the position of the ship is given in Figure 1. On average, the air parcels are initialized 5.3 days before arriving at the ship. The specific humidity of the parcel is initially taken from the trajectory data set and then modeled prognostically.

Along the trajectory, the specific humidity and isotopic composition of the parcel can increase or decrease due to the surface flux and decrease due to cloud formation. If the air parcel moves above the ABL, only cloud formation may influence the isotopic composition of the parcel (Figure 2). As soon as the parcel enters the ABL again, the model considers both cloud formation and the surface flux. Assuming a well-mixed ABL with a height-constant vapor density, the moisture flux into or out of the parcel (J_a) due to the surface flux (J) is computed as

$$J_a = J \frac{d_a}{d_{ABL}}, \tag{1}$$

where $d_a = 1$ m and d_{ABL} are the depths of the air parcel and ABL, respectively. The specific humidity in Model Air Parcel agrees approximately with that in the trajectory data set (Figure S3 in Supporting Information S1). Considering all data points from the initialization of the air parcels to the arrival at the ship, the specific humidity in Model Air Parcel is characterized by a RMSE of 0.6 g kg^{-1} and a correlation coefficient of $\rho = 0.94$ when compared with the trajectory data set. Comparing only the values at the final position of the air parcels (i.e., at the ship) with the trajectory data set, specific humidity tends to be underestimated with RMSE = 0.9 g kg^{-1} and $\rho = 0.45$.

The isotopic composition of the sublimation flux is taken from Model Sublimation whereas the isotopic composition of the deposition flux is assumed to be in isotopic equilibrium with the air parcel. Consequently, the isotopic composition of the deposition flux can differ between Model Air Parcel and Model Sublimation as the latter uses a simpler estimate based on idealized vapor origins. In the case of vapor deposition, condensation, or ocean evaporation, the isotopic composition of the vapor exchanged between the surface and the air parcel depends and feeds back on the air parcel's isotopic composition (Text S3 in Supporting Information S1). To guarantee an accurate feedback, the time step needs to be small enough, especially if the vapor mass taken up or removed from the air parcel is in the same order of magnitude as the vapor mass contained in the parcel. Therefore, the effects of ocean evaporation, condensation, or vapor deposition are computed stepwise by dividing each 3-hr time step into 32 subintervals of equal length. This value was justified using an example situation, for which the number of subintervals was continuously increased by a factor of two until the isotopic composition of the parcel at the end

of the 3-hr step changed by less than 1%. An uncertainty in the order of 1% due to the temporal discretization is acceptable, considering that other model assumptions, for example, about the snowfall isotopic composition in Model Sublimation, lead to higher uncertainties.

Cloud formation occurs as soon as the specific humidity of the air parcel exceeds its saturation value. Isotopic fractionation during cloud formation is calculated using the classic Rayleigh distillation model with equilibrium fractionation (Jouzel & Merlivat, 1984; Sinclair et al., 2011). In this model, the cloud water precipitates immediately. In reality, the air is supersaturated in mixed-phase clouds and therefore, kinetic fractionation is expected to occur. Although this kinetic effect may be relevant for reproducing measurements of d-excess (Jouzel & Merlivat, 1984), we neglect this effect because the supersaturation ratio is a poorly constrained parameter and our analysis focuses on the less sensitive δ^{18}O values. The equilibrium fractionation factors used in the Rayleigh model are computed as in Sinclair et al. (2011), accounting for mixed-phase clouds with a gradual, linear shift from the vapor-liquid to the vapor-ice transition as the air temperature decreases from 0 to $-20°$C. Changes in air density along the trajectory influence the vapor mass contained in the parcel as they imply exchange of air with the surrounding atmosphere. The model assumes that this exchange of air does not have a direct effect on the isotopic composition of the parcel.

2.3. Data From the COSMO$_{iso}$ Model

Thurnherr, Jansing, et al. (2020) published regional high-resolution simulations with the isotope-enabled GCM COSMO$_{iso}$, covering parts of the Southern Ocean and Antarctic Ice Sheet during the ACE expedition. We compare vapor isotopic data from one of these simulations with the results of Model Air Parcel. While methodological details of the COMOiso simulation are described by the aforementioned authors and Thurnherr et al. (2021), we summarize the features that are most important for our comparison. The horizontal grid spacing (0.125°) is half of that for the ERA5 data and the model includes 40 vertical levels. Isotopic fractionation during ocean evaporation is modeled using the Craig-Gordon formula with a simple parameterization of the kinetic fractionation factor according to Pfahl and Wernli (2009). The snowpack is represented by a one-layer surface snow model. For snow sublimation, the COSMO$_{iso}$ model considers equilibrium fractionation.

From the COSMO$_{iso}$ simulation called leg2_run1, we extract specific humidity and the specific water vapor contents of H$_2^{18}$O and HD^{16}O at the lowest model level in the grid cell containing the position of the ship. This model level corresponds approximately to the measurement height. The vapor isotopic compositions for the COSMO$_{iso}$ simulation are computed as

$$\delta_i = \frac{q_i}{q} - 1 \qquad (2)$$

and expressed in ‰, where q is specific humidity and q_i is the specific water vapor content of a heavy water isotopologue divided by the isotopic ratio of the Vienna Standard Mean Ocean Water.

3. Results and Discussion

As expected, the simulated dynamics of δ^{18}O and δD are very similar. Therefore, we only present results for δ^{18}O and briefly discuss d-excess.

3.1. Comparison of Modeled and Measured Vapor Isotopic Compositions

Figure 3 compares the ensemble averaged vapor δ^{18}O and d-excess of the air parcels with the measurements on the ship close to the Mertz glacier. We show the baseline simulations using the relationship of Stenni et al. (2016) to parameterize the snowfall isotopic composition in Model Sublimation. For comparison, the figure includes results from the Eulerian model COSMO$_{iso}$, published by Thurnherr, Jansing, et al. (2020).

Similar to the measurements, our model predicts vapor δ^{18}O values at the ship of approximately $-15‰$ in the beginning and at the end of the investigated 6-day period and a pronounced minimum in the middle of the period. In the simulation considering equilibrium fractionation (Run E), this minimum is more pronounced (δ^{18}O $= -40‰$), compared to the simulation neglecting fractionation during snow sublimation (Run N, δ^{18}O $= -34‰$). Differences between both model runs are mainly visible in the middle of the study period. Overall, both runs achieve
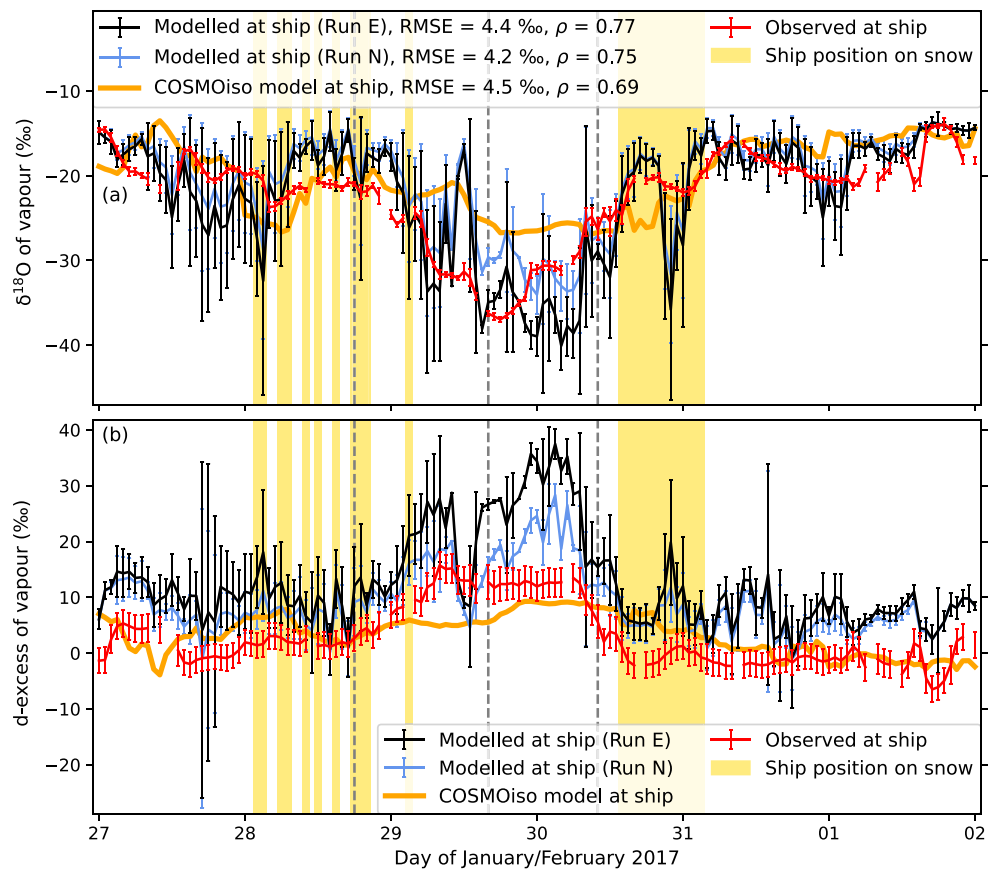
Figure 3. Modeled and measured (a) δ^{18}O and (b) d-excess of atmospheric water vapor at the ship close to the Mertz glacier from 27 January to 1 February 2017. We show the modeled ensemble averages and standard deviations for multiple air parcels in the baseline simulations. The measurements represent 1-hr mean values and standard deviations. In the legend, root-mean-square errors (RMSE) and Pearson correlation coefficients (ρ) are specified for the model-measurement comparison. The yellow shading indicates times when the ship was located in a grid cell modeled as snow-covered land; at the other times, the ship was in a grid cell treated as ice-free ocean. The vertical gray dashed lines indicate times analyzed in Figure 5.

a similar agreement with the measurements with root-mean-square errors (RMSE) of 4.4 and 4.2‰ and Pearson correlation coefficients of 0.77 and 0.75 for Run E and Run N, respectively.

In a few short periods, we observe strong deviations of up to ±15‰ between the modeled and measured δ^{18}O values. Run E predicts clearly too depleted vapor isotopic compositions on 28 January around 03:00 and in the earliest and latest hours of 30 January. On the contrary, the modeled isotopic composition is clearly too enriched on 29 January around 12:00. As will be shown later, the cases with too depleted isotopic compositions occur at times when the air parcels have experienced a substantial influence of snow sublimation along their trajectories, which is also visible from the noticeable difference between Run E and Run N. Therefore, it is likely that the isotopic composition of the surface snow is biased, at least in certain areas. This problem can arise from uncertainties in the δ-temperature relationship for snowfall, applied in Model Sublimation. Figure S4 and Text S5 in Supporting Information S1 show that the lowest δ^{18}O values at the ship are sensitive with respect to the δ-temperature relationship. With the relationships of Fujita and Abe (2006) and Landais et al. (2012), the lowest vapor δ^{18}O values are approximately 5‰ higher and lower, respectively, compared to the baseline simulation. Therefore, the generalization of a site-specific, empirical δ-temperature relationship for snowfall is a strong simplification in the model and contributes to deviations between the model and the measurements. All three δ-temperature relationships tested in this study characterize high-elevation sites on the Antarctic plateau where the temperatures are low and the distillation effect drives the isotopic composition of the snowfall. In coastal areas, however, the snowfall isotopic composition is expected to depend additionally on the humidity conditions in the vapor source region (Touzeau et al., 2016), which is neglected in Model Sublimation. Furthermore, the

δ-temperature relationships become more uncertain when applied to temperatures outside the range observed at the high-elevation sites.

Another important source of uncertainty is the simplified representation of sea ice. Air parcels taking up moisture from the surface of grid cells with a sea ice cover below the applied threshold of 90% only experience the effect of ocean evaporation in the model while in reality, a part of the moisture uptake is caused by sublimation of snow or ice with a depleted isotopic composition, compared to the liquid ocean water. Additionally, the isotopic composition of sublimating snow on top of sea ice may be influenced by sea spray, which is neglected in the model.

Moreover, the coarse spatial resolution may contribute substantially to the model-measurement deviations as the coastline is not accurately represented. The model may overestimate or underestimate the time spent by the air parcels in the marine ABL shortly before arriving at the ship, depending on whether the ship is located in a grid cell treated as ice-free ocean or snow surface (yellow shading in Figure 3). If an air parcel with a strongly depleted δ^{18}O value reaches the coast and takes up moisture from the ice-free ocean, the isotopic signature of the parcel can change abruptly as the evaporation flux is much more enriched in heavy SWIs than the air parcel. This effect is particularly strong due to kinetic fractionation, which is driven by the vertical gradients of the water isotopologues above the ocean surface. For an air mass with a very depleted δ^{18}O value, the abundance of the heavy isotopologue will decrease strongly with height above the ocean surface, which enhances the evaporation of the heavy isotopologue. In extreme cases, this kinetic effect can outweigh the effect of equilibrium fractionation such that the evaporation flux can be more enriched in SWIs than the ice-free ocean (Equation 13 in Supporting Information S1). As the air parcel spends more time in the ABL over the ice-free ocean, the parcel's isotopic composition becomes more similar to that of the ocean and the kinetic effect is generally less pronounced than before.

Further sources of uncertainty with probably minor impacts on the vapor δ^{18}O values may be (a) a bias in the initial isotopic composition of air parcels over the ocean due to the global closure assumption or a bias in the surface water δ^{18}O; (b) the neglect of kinetic fractionation during cloud formation; (c) the neglect of mixing of air masses with different isotopic compositions, for example, at weather fronts; (d) uncertainties of the ABL height provided with the trajectory data set, influencing the modeled time period and magnitude of moisture exchange between the air parcels and the surface; and (e) the simple assumption that the vapor mass exchanged between the atmosphere and the surface is homogeneously distributed between the surface and the ABL height (Equation 1). This last assumption neglects the fact that, even in a perfectly mixed ABL, an air parcel located close to the surface would take up slightly more mass of vapor from the evaporation or sublimation flux than a parcel at a greater height because the air density decreases with height. The assumption of a perfectly mixed ABL could be implemented more rigorously by considering the mass ratio instead of the thickness ratio for the air parcel and the ABL in Equation 1. Yet, this choice only has a minor effect on our analysis as the ABL height is generally small (780 m on average). Additionally, the air in the ABL is not always perfectly mixed, especially in a stable ABL.

Although there are some hours with a large model-measurement mismatch, Model Air Parcel is able to reproduce the general trend and timing of the vapor depletion event on 29 and 30 January 2017. This depletion event is less visible in the δ^{18}O time series extracted from the COSMO$_{iso}$ simulation, which predicts a minimum δ^{18}O that is 10‰ more enriched, compared to the measurements (Figure 3a). This mismatch may be related to the fact that the snowpack is represented as a single layer with vertically homogeneous isotopic compositions in the COSMO$_{iso}$ model. As demonstrated with a sensitivity analysis for Model Sublimation (Text S4, Figure S1 in Supporting Information S1), the seasonal and shorter-term variability of the snow isotopic composition decreases significantly with increasing thickness of the considered snow layers.

The measured d-excess of water vapor at the ship is mostly close to zero in the first two and last two days of the study period and exhibits higher values of approximately 13‰ in the middle of the period when the most depleted isotopic compositions are reached (Figure 3b). Our model generally overestimates the measured d-excess values, especially for Run E in the middle of the study period (maximum d-excess: 37‰). Some disagreement between the modeled and measured d-excess is expected, given the poor representation of kinetic fractionation. Future work could improve the model by parameterizing kinetic fractionation during cloud formation using the semi-empirical approach of Jouzel and Merlivat (1984). Additionally, the d-excess of snowfall in Model Sublimation is uncertain because it is based on the δD-δ^{18}O relationship derived by Masson-Delmotte et al. (2008) from a variety of samples including snowfall, snow pits, firn cores, and ice cores, which may partly be influenced by postdepositional processes such as sublimation. Compared to our model, the COSMO$_{iso}$ model performs better in reproducing the measured d-excess although the maximum d-excess is slightly underestimated by the COSMO$_{iso}$

simulation (Figure 3b). Due to the limitations of our model with respect to d-excess, the remaining analysis focuses on the δ^{18}O signal.

3.2. Drivers of the Vapor Isotopic Composition

Previous studies at other coastal polar sites have found distinct isotopic signatures for air masses advected from the ocean and those advected from the ice sheet (e.g., Bréant et al., 2019; Kopec et al., 2014; Kurita et al., 2016a, 2016b). Therefore, it is a plausible hypothesis that shifts between such air masses largely explain the observed isotope dynamics close to the Mertz glacier. The more depleted isotopic composition and higher d-excess of vapor over the ice sheet is generally thought to result from the distillation effect of cloud formation with contributions from both equilibrium and kinetic fractionation (Jouzel & Merlivat, 1984; Kurita et al., 2016a; Masson-Delmotte et al., 2008). However, the sublimation and deposition fluxes including isotopic fractionation also influence the variability of the vapor isotopic signal. As the ocean is often a strong vapor source, the distance between the ship and the ice sheet or sea ice may play an important role. In the marine boundary layer, a strong vertical humidity gradient, typically associated with cold air advection over a relatively warm ocean surface, leads to strong evaporation with enhanced kinetic fractionation. This effect can cause differences of several ‰ in the vapor δ^{18}O between cold and warm sectors of extratropical cyclones but it is unlikely to explain a large decrease of more than 10‰ (Thurnherr et al., 2021). We now investigate which of the aforementioned drivers play a dominant role in our case study.

On the first day and during most of the last 2 days of the study period, the ship moved towards and away from the ice sheet, respectively (Figure 1). Due to a longer distance to the ice sheet, it is likely that recent ocean evaporation caused the relatively enriched vapor δ^{18}O at this time. From 28 January 2017, 02:00, to 31 January 2017, 06:00, the ship stayed in close proximity to the ice sheet. In this phase, the δ^{18}O remained relatively enriched for one day and then dropped to very depleted values. The fact that only the most depleted δ^{18}O values and the highest d-excess values in the time series are sensitive with respect to assumptions in Model Sublimation (Figure 3 and Figure S4 in Supporting Information S1) is consistent with the hypothesis that processes over the ocean drove the vapor isotopic composition in the first and last two days of the period while processes over the Antarctic Ice Sheet influenced the isotopic signature in the middle of the period.

Moreover, the rather small differences between Runs E and N demonstrate that isotopic fractionation during snow sublimation can only explain a small part of the minimum in the δ^{18}O time series. Regarding d-excess, the difference between Runs E and N shows that equilibrium fractionation during sublimation influences the modeled d-excess. This influence is caused by the fact that the δD-δ^{18}O slope associated with equilibrium fractionation amounts to a value lower than 8 at very depleted isotopic compositions and low temperatures (e.g., Dütsch et al., 2017; Touzeau et al., 2016). For the same reason, the modeled d-excess is also influenced by other processes such as vapor deposition and cloud formation, which are represented assuming equilibrium fractionation. Consequently, the increased d-excess values in the middle of the study period do not necessarily reflect an influence of kinetic fractionation.

The initial isotopic composition of the air parcels can influence the model results, especially if the time between initialization and arrival at the ship is short. Air parcels initialized over the ocean start their trajectories with fairly uniform δ^{18}O values between approximately −17‰ and −11‰ (Figure 4a). These initial values are similar to the final isotopic composition modeled at the ship during the first two and last 2 days of the investigation period, suggesting that ocean evaporation is an important driver. As expected, air parcels initialized over snow have more variable and more depleted initial δ^{18}O values than those initialized over ocean. Interestingly, there are almost always some air parcels that are initialized over snow and the range of their initial δ^{18}O values remains similar throughout the period (approximately −70‰ to −40‰ in Run E). However, when the most depleted δ^{18}O values are observed at the ship, almost all air parcels are initialized over snow. This fact supports the hypothesis that the air masses originate from the interior of the ice sheet at this time.

To assess the importance of different moisture exchange processes along the trajectories, we show in Figure 4b the ensemble-averaged relative contribution of specific processes to the total absolute exchange of moisture mass between an air parcel and the surrounding. Moisture uptake from the ocean is relevant throughout the study period and often represents the process with the strongest contribution to the total moisture exchange. The contribution of moisture uptake from snow surfaces is variable in time and becomes highest when the modeled vapor isotopic composition at the ship is most depleted and sometimes significantly more depleted than the measured values (Figures 3a and 4b). In most of these cases, moisture uptake from the snow surface contributes more than
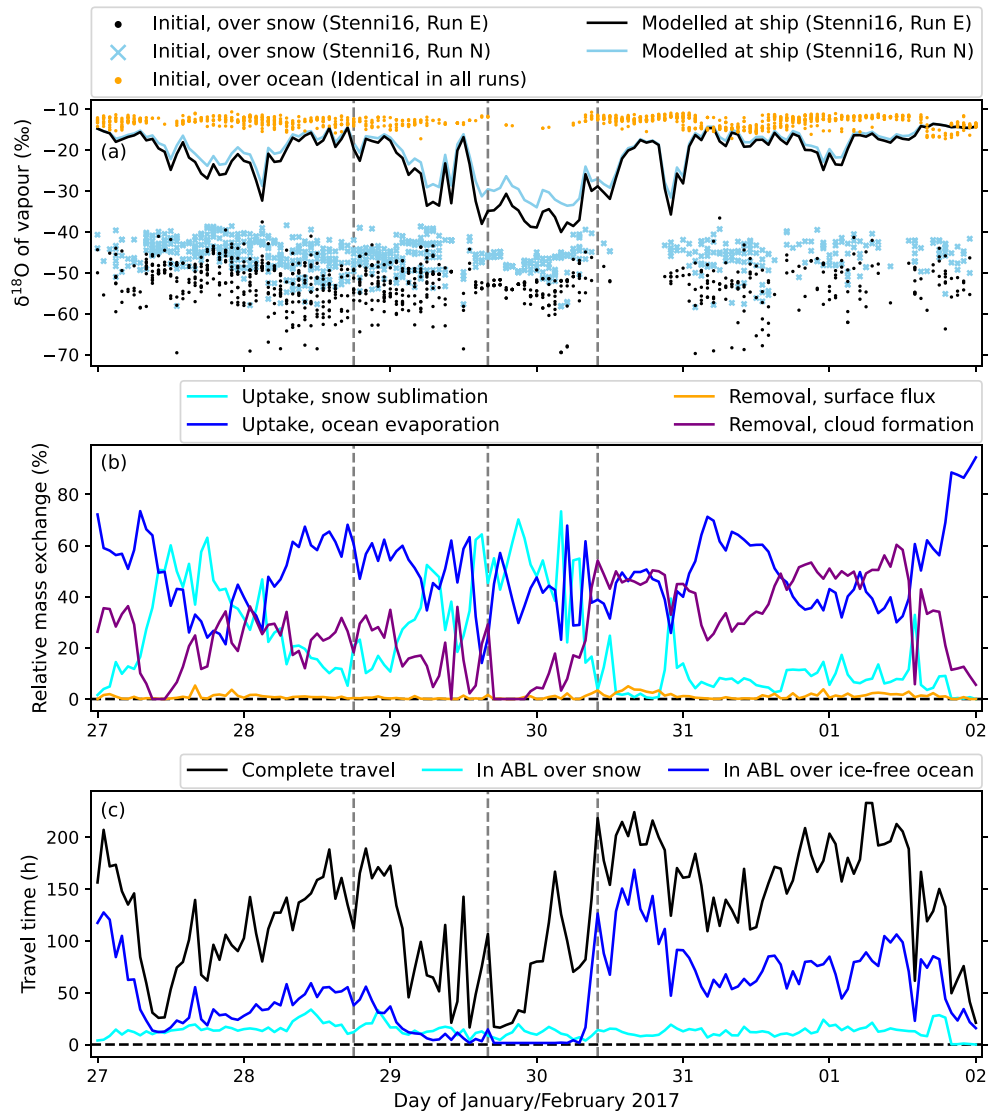
Figure 4. (a) Comparison between initial $\delta^{18}O$ of individual air parcels and ensemble-averaged final $\delta^{18}O$ at the ship; (b) Ensemble average of the relative exchange of moisture mass between an air parcel and the surrounding due to different processes between initialization and arrival at the ship; the sum of the displayed values is 100% at each time; (c) Average travel time of the air parcels and average times spent in the atmospheric boundary layer (ABL) over snow-covered land or sea ice and the ABL over the ice-free ocean. The vertical gray dashed lines indicate times analyzed in Figure 5.

any other process to the total moisture exchange. Moisture removal due to cloud formation is a relevant process for most of the time but plays a minor role in the middle of the study period when sublimation is the dominating process. Overall, the contribution of cloud formation to the total moisture exchange correlates strongly with the travel time of the air parcels, that is, the time between initialization and arrival at the ship (Figures 4b and 4c). This correlation reflects the fact that a longer travel time increases the probability for air mass lifting and cooling. Vapor removal due to the surface flux generally represents the smallest term in the moisture budget with a relative contribution of no more than 5%.

Although the parcels experience little cloud formation in the middle of the period, the distillation effect of cloud formation may still be responsible for the very depleted $\delta^{18}O$ values as this effect influences indirectly the initial isotopic composition of air parcels, which begin their trajectory over the interior of the ice sheet. More precisely, the initial isotopic composition of a parcel over snow depends on the snowfall isotopic composition, which decreases with lower air temperatures, reflecting more isotopic distillation due to a larger temperature difference between the ocean (typical vapor source) and the air parcel.
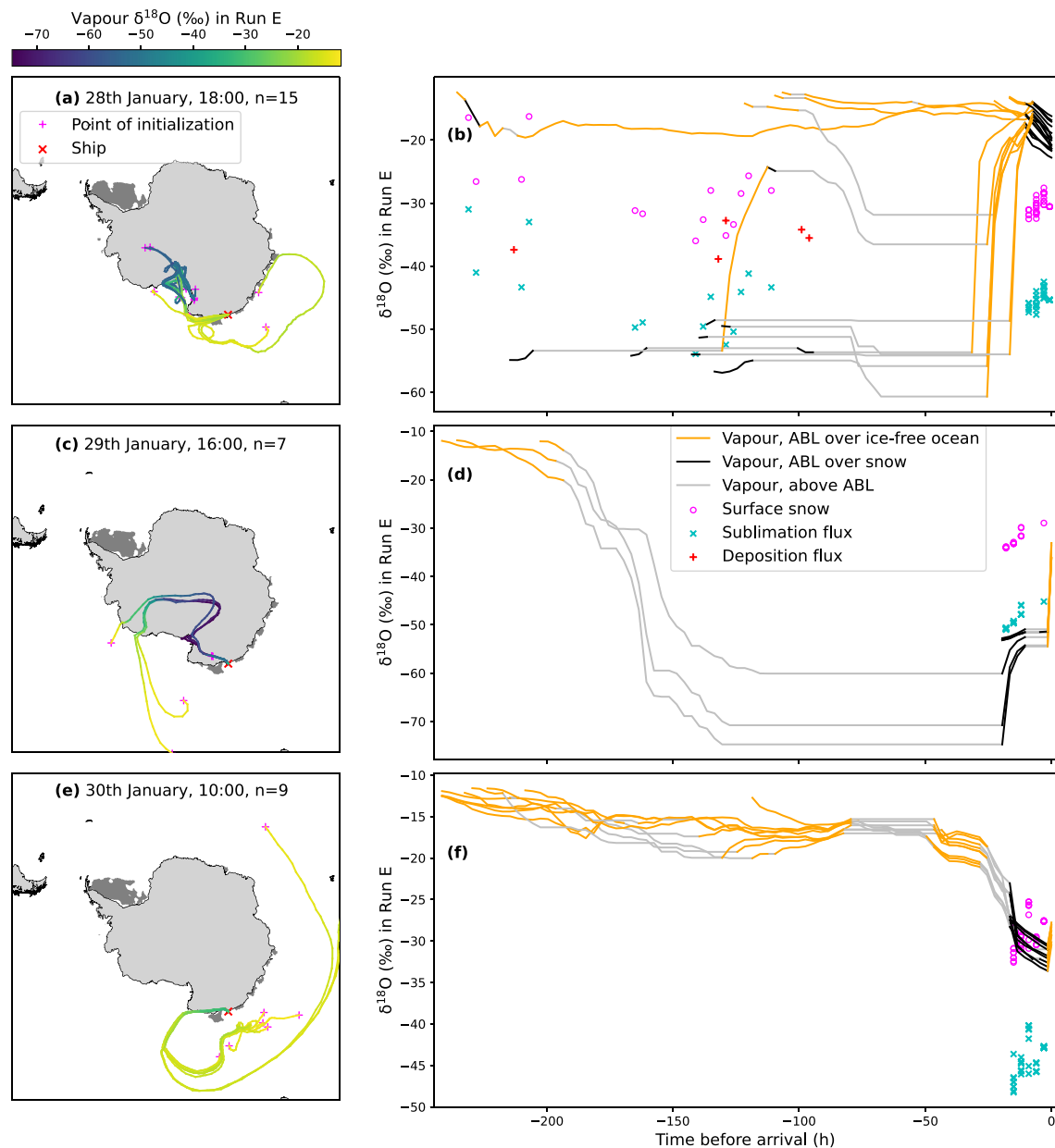
Figure 5. Vapor δ^{18}O along air parcel trajectories in the baseline simulation of Run E for three different times of arrival at the ship (gray dashed lines in Figures 3 and 4). (a, c, and e) Each of the three cases is illustrated with a map and (b, d, and f) δ^{18}O-time diagram. The number of trajectories is denoted by n and areas treated as snow-covered sea ice are colored dark gray in the maps. The surface snow and sublimation flux are only shown in panels (b, d, and f) when sublimation affects the air parcel. Trajectories arriving at the ship at a lower height are plotted on top of others.

In the middle of the study period, the air parcels spend very little time in the ABL over the ice-free ocean (at times only in the last time step) while they spend more time in the ABL over snow-covered land or sea ice (Figure 4c). Overall, Figures 3 and 4 show that the air masses with the most depleted δ^{18}O values and the highest d-excess values originate from the ice sheet and their isotopic signature is influenced by snow sublimation. This isotopic signature seems to only reach the ship if the air masses spend little time in the ABL over the ice-free ocean shortly before their arrival such that ocean evaporation cannot overwrite the signature.

To better understand which drivers act in which sections of the air parcel trajectories, we illustrate the δ^{18}O values along individual trajectories in space and time for three different arrival times in Figure 5. The arrival times include situations with relatively enriched and depleted δ^{18}O values while the ship is close to the ice sheet, the ensemble averaged travel time of the air parcels is at least 4 days, and the modeled vapor δ^{18}O only deviates

slightly from the measured one. Figures 5a and 5b show a situation leading to relatively enriched δ^{18}O values at the ship. In this case, the air parcels travel some distance in the ABL over the ice-free ocean parallel to the Antarctic coast before moving in the ABL over a snow-covered area in the last 10 hr of their travel. Almost half of the air parcels are initialized over the ice sheet and exhibit strongly depleted δ^{18}O values around −52‰ until they enter the ABL over the ice-free ocean. Due to ocean evaporation, the δ^{18}O of the air parcels quickly increases and reaches values comparable to those of parcels initialized over the ocean.

Figures 5c and 5d refer to a situation with one of the most depleted δ^{18}O values measured at the ship. Four of seven air parcels are initialized over the ice sheet and take a direct and short route to the ship where they only take up moisture from the ice-free ocean in the last time step. Their final δ^{18}O values are similar to those of the other three parcels that are initialized over the ocean and travel over the interior of the ice sheet before taking the same final route as the parcels initialized over snow. While the parcels are lifted over the ice sheet and above the ABL, their isotopic composition becomes increasingly depleted due to the distillation effect of cloud formation and reaches extreme δ^{18}O values of approximately −60‰ to −75‰. After reaching these extreme values, the air parcels maintain their isotopic composition for approximately 4 days because cloud formation stops as soon as the parcels begin to descend and the surface flux does not affect the free troposphere above the ABL. Only towards the end of the trajectories as the parcels move over the escarpment zone of the ice sheet, they enter the ABL over snow. At this time, approximately 20 hr before the arrival at the ship, snow sublimation adds vapor with a relatively enriched δ^{18}O value to the parcels (Figure 5d). The sublimation flux in the escarpment zone is relatively enriched in heavy SWIs compared to the air parcels because their isotopic composition was shaped at higher and colder levels over the interior of the ice sheet. Additionally, the parcel isotopic composition is particularly sensitive with respect to moisture uptake after most of the initial vapor mass was removed from the parcels due to cloud formation. As a consequence, the moisture uptake in the escarpment zone increases the isotopic composition of the parcels abruptly. This increase caused by sublimation is similarly strong as another increase in the last time step, when the parcels reach the ice-free ocean and take up moisture from the water surface.

The situation shown in Figures 5e and 5f leads to an intermediate δ^{18}O at the ship. All air parcels start their trajectories over the ocean and finally travel over the coastal zone of the ice sheet. Already over the ocean, cloud formation and condensation at the surface begin to decrease the δ^{18}O of the parcels. As soon as the parcels reach the ice sheet, their δ^{18}O continues to decrease because snow sublimation adds vapor with a more depleted δ^{18}O value to the air parcels. In this situation, the sublimation flux is more depleted in heavy SWIs compared to the parcels because the latter carry the isotopic signature of processes over the ocean.

4. Conclusions

We developed a Lagrangian isotope model with the aim to reproduce and explain the vapor δ^{18}O time series measured on the ACE ship close to the Mertz glacier in a 6-day period in austral summer 2017. The vapor mass and isotopic composition of air parcels was modeled along trajectories between an initial location in the ABL and the final location in the ABL at the ship. While isotope effects of cloud formation and ocean evaporation were represented with common approaches (classic Rayleigh distillation model and Craig-Gordon formula, respectively), the effect of snow sublimation was estimated using a novel approach, considering changes of the isotopic composition in a multi-layer snowpack due to snowfall, sublimation, and vapor deposition.

Similar to the measured values, the modeled vapor δ^{18}O at the ship reaches a pronounced minimum value of −40‰ in the middle of the study period. The RMSE of the baseline simulation amounts to 4.4‰, which is reasonable considering the model limitations such as the generalization of a site-specific δ^{18}O-temperature relationship for snowfall and the strongly simplified representation of snow on top of sea ice. Our analysis confirms the hypothesis that the relatively enriched δ^{18}O values are associated with air masses advected from the ocean whereas the strongly depleted δ^{18}O values are caused by direct advection of air masses from the Antarctic Ice Sheet. This result is consistent with similar observations at other coastal polar sites in the literature. As expected, cloud formation leads to very depleted vapor isotopic compositions over the ice sheet. Snow sublimation can also significantly modify the isotopic composition of the air parcels depending on their origin. For example, air parcels originating from high levels over the interior of the ice sheet may carry a strongly depleted isotopic signature to the escarpment zone of the ice sheet and then experience an abrupt and strong enrichment in heavy SWIs due to a relatively enriched sublimation flux. The model run considering equilibrium fractionation during snow sublimation leads to a more pronounced minimum in the vapor isotopic composition at the ship, compared

with the model run neglecting fractionation during sublimation. Although the latter model run agrees slightly better with the measured isotopic composition at the ship, snow sublimation may still be associated with fractionation as the model-measurement agreement is also influenced by the other model uncertainties. A critical factor for the vapor $\delta^{18}O$ at the ship is the time that the air parcels spend in the marine ABL shortly before arriving at the ship because ocean evaporation can quickly overwrite their isotopic signature.

Our modeling approach could be adapted for a study similar to Helsen et al. (2006) to simulate the vertical isotope profile in snow pits using backward trajectories for events of snow accumulation at an Antarctic site and deriving the isotopic composition of local snowfall from that of the air parcels. In contrast to the model of Helsen et al. (2006), our model accounts for the postdepositional effects of snow sublimation and vapor deposition. However, further improvements in our model such as the parameterization of kinetic fractionation during cloud formation and snow-atmosphere exchange as well as a more sophisticated vapor transport mechanism in the snowpack may be important for this purpose. Moreover, the deposition of drifting and blowing snow can contribute to snow accumulation and influence the isotopic composition of surface snow. To understand the latter effect, fundamental research is needed as the isotopic composition of drifting and blowing snow particles may be altered by sublimation, which has not been studied so far.

Conflict of Interest

The authors declare no conflicts of interest relevant to this study.

Data Availability Statement

Model results were generated using Copernicus Climate Change Service information (2021) available at https://doi.org/10.24381/cds.adbb2d47 (Hersbach et al., 2018). The air parcel trajectories were downloaded from https://doi.org/10.5281/zenodo.4031705 (Thurnherr, Wernli, & Aemisegger, 2020). The calibrated isotope measurements from the ACE campaign were downloaded from https://doi.org/10.5281/zenodo.3250790 (Thurnherr & Aemisegger, 2020). Simulation data of the COSMO$_{iso}$ model were downloaded from https://doi.org/10.3929/ethz-b-000445744 under the CC BY 4.0 license available at https://creativecommons.org/licenses/by/4.0/ (Thurnherr, Jansing, et al., 2020). Validation data from the Dome C site containing $\delta^{18}O$ of surface snow and atmospheric vapor were retrieved from https://doi.org/10.5194/tc-12-1745-2018-supplement and https://doi.org/10.5194/acp-16-8521-2016-supplement, respectively (Casado et al., 2016, 2018). The python programming code and the main model output including the data shown in the figures are available at https://doi.org/10.16904/envidat.417 (Sigmund et al., 2023). The figures were made with Matplotlib version 3.5.1, available under the Matplotlib license at https://matplotlib.org/.

References

Akers, P. D., Kopec, B. G., Mattingly, K. S., Klein, E. S., Causey, D., & Welker, J. M. (2020). Baffin Bay sea ice extent and synoptic moisture transport drive water vapor isotope ($\delta^{18}O$, δ^2H, and deuterium excess) variability in coastal northwest Greenland. *Atmospheric Chemistry and Physics*, *20*(22), 13929–13955. https://doi.org/10.5194/acp-20-13929-2020

Bonne, J.-L., Behrens, M., Meyer, H., Kipfstuhl, S., Rabe, B., Schönicke, L., et al. (2019). Resolving the controls of water vapour isotopes in the Atlantic sector. *Nature Communications*, *10*(1), 1632. https://doi.org/10.1038/s41467-019-09242-6

Bréant, C., Dos Santos, C. L., Agosta, C., Casado, M., Fourré, E., Goursaud, S., et al. (2019). Coastal water vapor isotopic composition driven by katabatic wind variability in summer at Dumont d'Urville, coastal East Antarctica. *Earth and Planetary Science Letters*, *514*, 37–47. https://doi.org/10.1016/j.epsl.2019.03.004

Casado, M., Landais, A., Masson-Delmotte, V., Genthon, C., Kerstel, E., Kassi, S., et al. (2016). Continuous measurements of isotopic composition of water vapour on the East Antarctic Plateau. *Atmospheric Chemistry and Physics*, *16*(13), 8521–8538. https://doi.org/10.5194/acp-16-8521-2016

Casado, M., Landais, A., Picard, G., Münch, T., Laepple, T., Stenni, B., et al. (2018). Archival processes of the water stable isotope signal in East Antarctic ice cores. *The Cryosphere*, *12*(5), 1745–1766. https://doi.org/10.5194/tc-12-1745-2018

Christner, E., Kohler, M., & Schneider, M. (2017). The influence of snow sublimation and meltwater evaporation on δD of water vapor in the atmospheric boundary layer of central Europe. *Atmospheric Chemistry & Physics*, *17*(2), 1207–1225. https://doi.org/10.5194/acp-17-1207-2017

Ciais, P., & Jouzel, J. (1994). Deuterium and oxygen 18 in precipitation: Isotopic model, including mixed cloud processes. *Journal of Geophysical Research*, *99*(D8), 16793–16803. https://doi.org/10.1029/94JD00412

Craig, H., & Gordon, L. I. (1965). Deuterium and oxygen 18 variations in the ocean and the marine atmosphere. In E. Tongiorgi (Ed.), *Stable Isotopes in Oceanographic Studies and Paleotemperatures* (pp. 9–130). Consiglio Nazionale delle Richerche, Laboratorio de Geologia Nucleare Pisa.

Cuffey, K. M., & Steig, E. J. (1998). Isotopic diffusion in polar firn: Implications for interpretation of seasonal climate parameters in ice-core records, with emphasis on central Greenland. *Journal of Glaciology*, *44*(147), 273–284. https://doi.org/10.3189/S0022143000002616

Dansgaard, W. (1964). Stable isotopes in precipitation. *Tellus*, *16*(4), 436–468. https://doi.org/10.3402/tellusa.v16i4.8993

Dar, S. S., Ghosh, P., Swaraj, A., & Kumar, A. (2020). Craig–Gordon model validation using stable isotope ratios in water vapor over the Southern Ocean. *Atmospheric Chemistry and Physics*, *20*(19), 11435–11449. https://doi.org/10.5194/acp-20-11435-2020

Dütsch, M., Pfahl, S., Meyer, M., & Wernli, H. (2018). Lagrangian process attribution of isotopic variations in near-surface water vapour in a 30-year regional climate simulation over Europe. *Atmospheric Chemistry and Physics*, *18*(3), 1653–1669. https://doi.org/10.5194/acp-18-1653-2018

Dütsch, M., Pfahl, S., & Sodemann, H. (2017). The impact of nonequilibrium and equilibrium fractionation on two different deuterium excess definitions. *Journal of Geophysical Research: Atmospheres*, *122*(23), 12732–12746. https://doi.org/10.1002/2017JD027085

Ebner, P. P., Steen-Larsen, H. C., Stenni, B., Schneebeli, M., & Steinfeld, A. (2017). Experimental observation of transient δ^{18}O interaction between snow and advective airflow under various temperature gradient conditions. *The Cryosphere*, *11*(4), 1733–1743. https://doi.org/10.5194/tc-11-1733-2017

ECMWF. (2016). IFS documentation CY41R2 – Part IV: Physical processes. In *IFS Documentation CY41R2*. https://doi.org/10.21957/tr5rv27xu

Elliot, T. (2014). Environmental tracers. *Water*, *6*(11), 3264–3269. https://doi.org/10.3390/w6113264

EPICA community members. (2004). Eight glacial cycles from an Antarctic ice core. *Nature*, *429*(6992), 623–628. https://doi.org/10.1038/nature02599

Friedman, I., Benson, C., & Gleason, J. (1991). Isotopic changes during snow metamorphism. In H. Taylor, J. O'Neil, & I. Kaplan (Eds.), *Stable Isotope Geochemistry: A Tribute to Samuel Epstein* (pp. 211–221). Geochemical Society.

Fujita, K., & Abe, O. (2006). Stable isotopes in daily precipitation at Dome Fuji, East Antarctica. *Geophysical Research Letters*, *33*(18), L18503. https://doi.org/10.1029/2006GL026936

Grootes, P., Steig, E., & Stuiver, M. (1994). Taylor Ice Dome study 1993–1994: An ice core to bedrock. *Antarctic Journal of the United States*, *29*, 79–81.

Helsen, M., Van de Wal, R., & Van den Broeke, M. (2007). The isotopic composition of present-day Antarctic snow in a Lagrangian atmospheric simulation. *Journal of Climate*, *20*(4), 739–756. https://doi.org/10.1175/JCLI4027.1

Helsen, M., Van de Wal, R., Van den Broeke, M., As, D. V., Meijer, H., & Reijmer, C. (2005). Oxygen isotope variability in snow from western Dronning Maud Land, Antarctica and its relation to temperature. *Tellus B: Chemical and Physical Meteorology*, *57*(5), 423–435. https://doi.org/10.1111/j.1600-0889.2005.00162.x

Helsen, M., Van de Wal, R., Van den Broeke, M., Masson-Delmotte, V., Meijer, H., Scheele, M., & Werner, M. (2006). Modeling the isotopic composition of Antarctic snow using backward trajectories: Simulation of snow pit records. *Journal of Geophysical Research*, *111*(D15), D15109. https://doi.org/10.1029/2005JD006524

Hersbach, H., Bell, B., Berrisford, P., Biavati, G., Horányi, A., Muñoz Sabater, J., et al. (2018). ERA5 hourly data on single levels from 1979 to present [Dataset]. Copernicus Climate Change Service (C3S) Climate Data Store (CDS). https://doi.org/10.24381/cds.bd0915c6

Hoffmann, G., Jouzel, J., & Masson, V. (2000). Stable water isotopes in atmospheric general circulation models. *Hydrological Processes*, *14*(8), 1385–1406. https://doi.org/10.1002/1099-1085(20000615)14:8⟨1385::AID-HYP989⟩3.0.CO;2-1

Horita, J., Rozanski, K., & Cohen, S. (2008). Isotope effects in the evaporation of water: A status report of the Craig–Gordon model. *Isotopes in Environmental and Health Studies*, *44*(1), 23–49. https://doi.org/10.1080/10256010801887174

Hughes, A. G., Wahl, S., Jones, T. R., Zuhr, A., Hörhold, M., White, J. W. C., & Steen-Larsen, H. C. (2021). The role of sublimation as a driver of climate signals in the water isotope content of surface snow: Laboratory and field experimental results. *The Cryosphere*, *15*(10), 4949–4974. https://doi.org/10.5194/tc-15-4949-2021

Jafari, M., Gouttevin, I., Couttet, M., Wever, N., Michel, A., Sharma, V., et al. (2020). The impact of diffusive water vapor transport on snow profiles in deep and shallow snow covers and on sea ice. *Frontiers in Earth Science*, *8*, 249. https://doi.org/10.3389/feart.2020.00249

Jancso, G., Pupezin, J., & Van Hook, W. (1970). Vapour pressure of H_2^{18}O ice (I) (−17°C to 0°C) and H_2^{18}O water (0°C to 16°C). *Nature*, *225*(5234), 723. https://doi.org/10.1038/225723a0

Johnsen, S. J., Dahl-Jensen, D., Gundestrup, N., Steffensen, J. P., Clausen, H. B., Miller, H., et al. (2001). Oxygen isotope and palaeotemperature records from six Greenland ice-core stations: Camp Century, Dye-3, GRIP, GISP2, Renland and NorthGRIP. *Journal of Quaternary Science: Published for the Quaternary Research Association*, *16*(4), 299–307. https://doi.org/10.1002/jqs.622

Joussaume, S., Sadourny, R., & Jouzel, J. (1984). A general circulation model of water isotope cycles in the atmosphere. *Nature*, *311*(5981), 24–29. https://doi.org/10.1038/311024a0

Jouzel, J., & Merlivat, L. (1984). Deuterium and oxygen 18 in precipitation: Modeling of the isotopic effects during snow formation. *Journal of Geophysical Research*, *89*(D7), 11749–11757. https://doi.org/10.1029/JD089iD07p11749

Jouzel, J., Vimeux, F., Caillon, N., Delaygue, G., Hoffmann, G., Masson-Delmotte, V., & Parrenin, F. (2003). Magnitude of isotope/temperature scaling for interpretation of central Antarctic ice cores. *Journal of Geophysical Research*, *108*(D12), 4361. https://doi.org/10.1029/2002JD002677

Koeniger, P., Leibundgut, C., Link, T., & Marshall, J. D. (2010). Stable isotopes applied as water tracers in column and field studies. *Organic Geochemistry*, *41*(1), 31–40. https://doi.org/10.1016/j.orggeochem.2009.07.006

Kopec, B., Lauder, A., Posmentier, E., & Feng, X. (2014). The diel cycle of water vapor in west Greenland. *Journal of Geophysical Research: Atmospheres*, *119*(15), 9386–9399. https://doi.org/10.1002/2014JD021859

Krinner, G., & Werner, M. (2003). Impact of precipitation seasonality changes on isotopic signals in polar ice cores: A multi-model analysis. *Earth and Planetary Science Letters*, *216*(4), 525–538. https://doi.org/10.1016/S0012-821X(03)00550-8

Kurita, N., Hirasawa, N., Koga, S., Matsushita, J., Steen-Larsen, H. C., Masson-Delmotte, V., & Fujiyoshi, Y. (2016a). Identification of air masses responsible for warm events on the East Antarctic coast. *SOLA*, *12*(0), 307–313. https://doi.org/10.2151/sola.2016-060

Kurita, N., Hirasawa, N., Koga, S., Matsushita, J., Steen-Larsen, H. C., Masson-Delmotte, V., & Fujiyoshi, Y. (2016b). Influence of large-scale atmospheric circulation on marine air intrusion toward the East Antarctic coast. *Geophysical Research Letters*, *43*(17), 9298–9305. https://doi.org/10.1002/2016GL070246

Landais, A., Ekaykin, A., Barkan, E., Winkler, R., & Luz, B. (2012). Seasonal variations of ^{17}O-excess and d-excess in snow precipitation at Vostok station, East Antarctica. *Journal of Glaciology*, *58*(210), 725–733. https://doi.org/10.3189/2012JoG11J237

Lorius, C., Merlivat, L., Jouzel, J., & Pourchet, M. (1979). A 30,000-yr isotope climatic record from Antarctic ice. *Nature*, *280*(5724), 644–648. https://doi.org/10.1038/280644a0

Majoube, M. (1970). Fractionation factor of ^{18}O between water vapour and ice. *Nature*, *226*(5252), 1242. https://doi.org/10.1038/2261242a0

Majoube, M. (1971). Fractionnement en oxygène 18 et en deutérium entre l'eau et sa vapeur. *Journal de Chimie Physique*, *68*, 1423–1436. https://doi.org/10.1051/jcp/1971681423

Masson-Delmotte, V., Hou, S., Ekaykin, A., Jouzel, J., Aristarain, A., Bernardo, R., et al. (2008). A review of Antarctic surface snow isotopic composition: Observations, atmospheric circulation, and isotopic modeling. *Journal of Climate*, *21*(13), 3359–3387. https://doi.org/10.1175/2007JCLI2139.1

Matsuo, S., & Matsubaya, O. (1969). Vapour pressure of H_2^{18}O ice. *Nature*, *221*(5179), 463–464. https://doi.org/10.1038/221463a0

Merlivat, L., & Jouzel, J. (1979). Global climatic interpretation of the deuterium-oxygen 18 relationship for precipitation. *Journal of Geophysical Research*, *84*(C8), 5029–5033. https://doi.org/10.1029/JC084iC08p05029

Merlivat, L., & Nief, G. (1967). Fractionnement isotopique lors des changements d'état solide-vapeur et liquide-vapeur de l'eau à des températures inférieures à 0°C. *Tellus*, *19*(1), 122–127. https://doi.org/10.1111/j.2153-3490.1967.tb01465.x

Neumann, T. A., & Waddington, E. D. (2004). Effects of firn ventilation on isotopic exchange. *Journal of Glaciology*, *50*(169), 183–194. https://doi.org/10.3189/172756504781830150

Noone, D., & Sturm, C. (2010). Comprehensive dynamical models of global and regional water isotope distributions. In J. B. West, G. J. Bowen, T. E. Dawson, & K. P. Tu (Eds.), *Isoscapes* (pp. 195–219). Springer. https://doi.org/10.1007/978-90-481-3354-3_10

Pfahl, S., & Wernli, H. (2009). Lagrangian simulations of stable isotopes in water vapor: An evaluation of nonequilibrium fractionation in the Craig-Gordon model. *Journal of Geophysical Research*, *114*(D20), D20108. https://doi.org/10.1029/2009JD012054

Pfahl, S., Wernli, H., & Yoshimura, K. (2012). The isotopic composition of precipitation from a winter storm – A case study with the limited-area model COSMO$_{iso}$. *Atmospheric Chemistry and Physics*, *12*(3), 1629–1648. https://doi.org/10.5194/acp-12-1629-2012

Schmale, J., Baccarini, A., Thurnherr, I., Henning, S., Efraim, A., Regayre, L., et al. (2019). Overview of the Antarctic Circumnavigation Expedition: Study of preindustrial-like aerosols and their climate effects (ACE-SPACE). *Bulletin of the American Meteorological Society*, *100*(11), 2260–2283. https://doi.org/10.1175/BAMS-D-18-0187.1

Sieber, M., Conway, T. M., de Souza, G. F., Hassler, C. S., Ellwood, M. J., & Vance, D. (2019). High-resolution Cd isotope systematics in multiple zones of the Southern Ocean from the Antarctic Circumnavigation expedition. *Earth and Planetary Science Letters*, *527*, 115799. https://doi.org/10.1016/j.epsl.2019.115799

Sigmund, A., Chaar, R., & Lehning, M. (2023). Modeled isotopic composition of water vapour along air parcel trajectories in the Antarctic [Dataset]. EnviDat. https://doi.org/10.16904/envidat.417

Sigmund, A., Dujardin, J., Comola, F., Sharma, V., Huwald, H., Melo, D. B., et al. (2022). Evidence of strong flux underestimation by bulk parametrizations during drifting and blowing snow. *Boundary-Layer Meteorology*, *182*(1), 119–146. https://doi.org/10.1007/s10546-021-00653-x

Sinclair, K. E., Marshall, S. J., & Moran, T. A. (2011). A Lagrangian approach to modelling stable isotopes in precipitation over mountainous terrain. *Hydrological Processes*, *25*(16), 2481–2491. https://doi.org/10.1002/hyp.7973

Sokratov, S. A., & Golubev, V. N. (2009). Snow isotopic content change by sublimation. *Journal of Glaciology*, *55*(193), 823–828. https://doi.org/10.3189/002214309790152456

Sprenger, M., & Wernli, H. (2015). The LAGRANTO Lagrangian analysis tool–version 2.0. *Geoscientific Model Development*, *8*(8), 2569–2586. https://doi.org/10.5194/gmd-8-2569-2015

Stenni, B., Scarchilli, C., Masson-Delmotte, V., Schlosser, E., Ciardini, V., Dreossi, G., et al. (2016). Three-year monitoring of stable isotopes of precipitation at Concordia Station, East Antarctica. *The Cryosphere*, *10*(5), 2415–2428. https://doi.org/10.5194/tc-10-2415-2016

Thurnherr, I., & Aemisegger, F. (2020). Calibrated data of stable water isotope measurements in water vapour at 13.5 m a.s.l., made in the austral summer of 2016/2017 around the Southern Ocean during the Antarctic Circumnavigation Expedition (ACE) [Dataset]. Zenodo. https://doi.org/10.5281/zenodo.3250790

Thurnherr, I., Hartmuth, K., Jansing, L., Gehring, J., Boettcher, M., Gorodetskaya, I., et al. (2021). The role of air–sea fluxes for the water vapour isotope signals in the cold and warm sectors of extratropical cyclones over the Southern Ocean. *Weather and Climate Dynamics*, *2*(2), 331–357. https://doi.org/10.5194/wcd-2-331-2021

Thurnherr, I., Jansing, L., Aemisegger, F., & Wernli, H. (2020). Numerical weather simulations using COSMO$_{iso}$ from December 2016–March 2017 along the ship track of the Antarctic Circumnavigation Expedition [Dataset]. ETH Zürich Research Collection. https://doi.org/10.3929/ethz-b000445744

Thurnherr, I., Kozachek, A., Graf, P., Weng, Y., Bolshiyanov, D., Landwehr, S., et al. (2020). Meridional and vertical variations of the water vapour isotopic composition in the marine boundary layer over the Atlantic and Southern Ocean. *Atmospheric Chemistry and Physics*, *20*(9), 5811–5835. https://doi.org/10.5194/acp-20-5811-2020

Thurnherr, I, Wernli, H., & Aemisegger, F. (2020). 10-day backward trajectories from ECMWF analysis data along the ship track of the Antarctic Circumnavigation Expedition in austral summer 2016/2017 [Dataset]. Zenodo. https://doi.org/10.5281/zenodo.4031705

Touzeau, A., Landais, A., Stenni, B., Uemura, R., Fukui, K., Fujita, S., et al. (2016). Acquisition of isotopic composition for surface snow in East Antarctica and the links to climatic parameters. *The Cryosphere*, *10*(2), 837–852. https://doi.org/10.5194/tc-10-837-2016

Town, M. S., Warren, S. G., Walden, V. P., & Waddington, E. D. (2008). Effect of atmospheric water vapor on modification of stable isotopes in near-surface snow on ice sheets. *Journal of Geophysical Research*, *113*(D24), D24303. https://doi.org/10.1029/2008JD009852

Wahl, S., Steen-Larsen, H. C., Reuder, J., & Hörhold, M. (2021). Quantifying the stable water isotopologue exchange between the snow surface and lower atmosphere by direct flux measurements. *Journal of Geophysical Research: Atmospheres*, *126*(13), e2020JD034400. https://doi.org/10.1029/2020JD034400

Wernli, B. H., & Davies, H. C. (1997). A Lagrangian-based analysis of extratropical cyclones. I: The method and some applications. *Quarterly Journal of the Royal Meteorological Society*, *123*(538), 467–489. https://doi.org/10.1002/qj.49712353811

Wever, N., Keenan, E., Amory, C., Lehning, M., Sigmund, A., Huwald, H., & Lenaerts, J. T. M. (2022). Observations and simulations of new snow density in the drifting snow-dominated environment of Antarctica. *Journal of Glaciology*, 1–18. https://doi.org/10.1017/jog.2022.102

References From the Supporting Information

Craig, H. (1961). Standard for reporting concentrations of deuterium and oxygen-18 in natural waters. *Science*, *133*(3467), 1833–1834. https://doi.org/10.1126/science.133.3467.1833

Gat, J. R., Mook, W. G., & Meijer, H. (2001). Environmental isotopes in the hydrological cycle: Principles and applications. *Technical Documents in Hydrology*, *2*(39).

Gat, J. R., Shemesh, A., Tziperman, E., Hecht, A., Georgopoulos, D., & Basturk, O. (1996). The stable isotope composition of waters of the eastern Mediterranean Sea. *Journal of Geophysical Research*, *101*(C3), 6441–6451. https://doi.org/10.1029/95JC02829

Kumar, B., & Nachiappan, R. P. (1999). On the sensitivity of Craig and Gordon Model for the estimation of the isotopic composition of lake evaporates. *Water Resources Research*, *35*(5), 1689–1691. https://doi.org/10.1029/1999WR900011

LeGrande, A. N., & Schmidt, G. A. (2006). Global gridded data set of the oxygen isotopic composition in seawater. *Geophysical Research Letters*, *33*(12), L12604. https://doi.org/10.1029/2006GL026011

Merlivat, L. (1978). Molecular diffusivities of $H_2^{16}O$, $HD^{16}O$, and $H_2^{18}O$ in gases. *The Journal of Chemical Physics*, *69*(6), 2864–2871. https://doi.org/10.1063/1.436884